

Midinfrared Optical Manipulation Based on Molecular Vibrational Resonance

Anna Statsenko, Yoshua Albert Darmawan^{ID}, Takao Fuji^{ID}, and Tetsuhiro Kudo^{ID*}

Laser Science Laboratory, Toyota Technological Institute, 2-12-1 Hisakata, Tempaku-ku, Nagoya 468-8511, Japan



(Received 30 March 2022; revised 1 September 2022; accepted 26 September 2022; published 15 November 2022)

Midinfrared light is extensively used for identifying molecules because their characteristic vibrational modes commonly exist in the midinfrared spectral region. In this paper, a midinfrared quantum cascade laser is utilized for sorting silica particles with resonant enhancement of the optical force by exciting their vibrational mode. Silica particles on an evanescent wave drift rapidly along the prism surface, whereas identical-sized polystyrene particles drift at 7–10 times lower speed. We suggest the application of this principle for optical force chromatography in the midinfrared region.

DOI: 10.1103/PhysRevApplied.18.054041

I. INTRODUCTION

Optical manipulation refers to the mechanical control of micro- and nanoscopic matter by lasers. It is an indispensable technique to further elevate the fundamental level of nanoscience and nanotechnology as Ashkin *et al.* revealed that particles suspended in solution are pushed [1] and trapped [2] by an optical force. In a plane propagating wave, the particles are pushed by a dissipative force (summation of the scattering force and absorption force) when the momentum of the photons is transferred to them through the light scattering and absorption processes [1]. In contrast, in optical tweezers [2], the particles are trapped at the center of a tightly focused laser beam by a gradient force. This can be interpreted as an induced polarization on the particle dragged along the electric field gradient. Recently, optical manipulation and trapping have been widely developed with various light fields such as plasmon-based locally enhanced electric fields [3,4], evanescent waves [5], ultrashort-pulsed lasers [6], and vortex beams [7].

The optical force can be drastically enhanced by the resonant interaction of a laser beam with the target matters through electronic transition resonance, which renders it possible to mechanically control matter according to their spectral information (anticipated application in optical force spectroscopy and optical force chromatography) [8–19]. In early reports, the Brownian motion of dye molecules, dye-doped nanoparticles, and dye-labeled antibodies were biased by resonant optical trapping [8, 9, 11, 12]. Recently, we had successfully observed significant resonance enhancement in trapping stiffness for a

single dye-doped polystyrene particle at an interface on irradiating with a trapping laser and a wide-field excitation laser [19]. Nevertheless, the dyes were unfortunately photobleached within a few tens of seconds, limiting practical usage. Consequently, photostable materials such as fluorescent nanodiamonds (NDs) are required for clear demonstration [17,18].

Remarkably, NDs with and without nitrogen-vacancy ($N-V$) centers were separated with a well-designed system using two different-colored counterpropagating laser beams. One laser is resonant, and another is nonresonant to the $N-V$ centers. It was realized by canceling the nonresonant optical force exerted on the ND itself with counterpropagating lasers. Then, the resonant optical force exerted on the $N-V$ centers becomes only the net driving force for pushing the NDs with $N-V$ centers to one side. For demonstrating the optical sorting, how to gain the more significant resonant force is another practical problem in addition to the photo-bleaching, which is the technical challenge in realizing optical force chromatography in the visible wavelength region.

Herein, we demonstrate optical force enhancement through molecular vibrational resonance using a midinfrared laser. The midinfrared range is a useful spectral range for identifying organic and inorganic molecules, proteins, and various nanomaterials because stronger vibrational modes can be detected in this range [20,21]. Molecular vibrational resonance is ubiquitous because most of the materials include vibrational modes. Additionally, the polarizability of many materials is considerable at the midinfrared wavelength, and they do not photobleach as compared to using electronic transition resonance. This is the report on optical manipulation in the midinfrared region, which enables the sorting of particles using a single propagating laser beam.

*kudo@toyota-ti.ac.jp

II. EXPERIMENT

We conduct an experiment in which a linearly polarized 9.3- μm quantum cascade laser (QCL, Thorlabs, 1075 cm^{-1} , single mode) is used for transporting the particles in the evanescent wave generated by total internal reflection with a ZnSe prism [see Fig. 1(a)]. The QCL is collimated by an aspheric lens (NA 0.85) and expanded approximately 4 times by a beam expander (focal lengths of each ZnSe lens are 50 and 200 mm). The resulting beam diameter is approximately 8 mm, and it is focused by the ZnSe lens (75-mm focal length) to the surface of a trapezoid ZnSe prism. The laser power before and after the prism is 151.2 and 99.3 mW. This decrease is due to the absorption of ZnSe material because the optical path length of the 9.3- μm laser in the prism is about a few centimeters. Therefore, we assume the laser power at the focus is 125 mW (we use this value for the theoretical calculation). The critical angle is 31.4° because the refractive indices of ZnSe and water at the 9.3- μm laser are 2.40 and 1.25, respectively [22,23]. We select a relatively large incident angle of 57° to suppress the water absorption by reducing the penetration depth (the calculated value is approximately 0.5 μm). For observing the laser pattern on the prism and particle images, an indium-tin-oxide (ITO) mirror is used for reflecting the infrared light and transmitting the visible light to their corresponding cameras. The visible scattering images are observed by using a reflective type objective lens (NA 0.5, Thorlabs) with a ring LED illuminator. For the smaller particles (1 and 2 μm), transmission images are recorded by using a water-immersion objective lens (NA 0.8, Olympus) under the illumination of a halogen lamp.

Inset in Fig. 1(a) is the infrared light pattern observed by an infrared camera (RIGI M2, Swiss TeraHertz) from the top of the prism. The vertical and horizontal diameters of the laser focus at the prism surface are approximately 100 and 200 μm , respectively. We consider that the 9.3- μm evanescent wave is scattered by the prism surface to the far field due to certain surface roughness, causing a random pattern. The focused beam profile without the prism is shown in Fig. 1(c). It shows a nice Gaussian distribution and the vertical and horizontal diameters are 170 and 153 μm , respectively. The elliptical shape is due to the QCL itself because the output laser divergence angles are slightly different in the vertical and horizontal directions. The moderate difference from the focal spot on the prism [the inset of Fig. 1(a)] may be caused by the refractive index of the ZnSe and incident angle. Figures 1(d) and 1(e) show scanning electron microscope images of the prism surface. There are scratches, blocks, and dots on the surface, which remain even after polishing the surface. The ZnSe is a relatively soft material compared to silica glass, and it is technically challenging to make the surface smooth. We suggest that the roughness is at least a few micrometers, which scatters the evanescent wave to the far

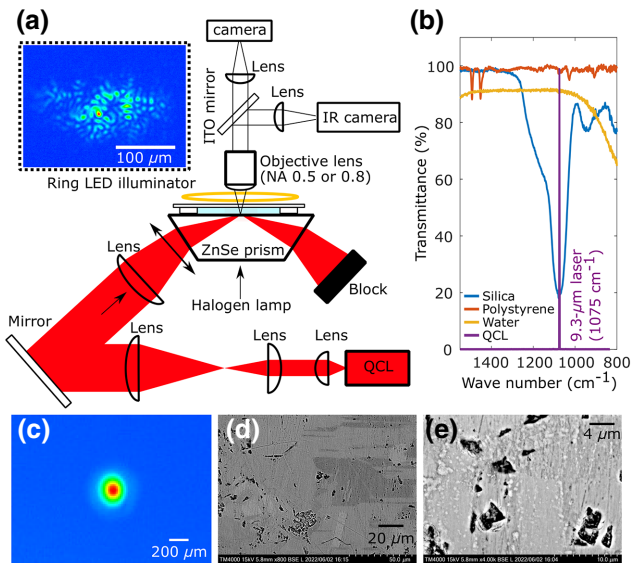


FIG. 1. (a) Optical setup for particle movement by the evanescent wave of the 9.3- μm QCL. The direction of linear polarization is denoted by the two-sided arrows. The dotted inset shows the spatial profile of the laser focused on the prism surface, measured by an IR camera. (b) Fourier-transform infrared spectra of silica particles, polystyrene particles, and water measured through the attenuated total reflection method. The purple line denotes the normalized spectrum of the 9.3- μm QCL. (c) Beam profile of the focused 9.3- μm laser measured by removing the prism. (d),(e) Scanning electron microscope images showing the ZnSe prism surface. The scales are denoted in each picture.

field. This prism is typically used as attenuated total reflection infrared spectral measurements for the bulk solution. Thereby the evanescent wave is generated on the surface. In the experiment, we select a relatively smoother surface than the other areas and check whether the particles drift at a nearly constant velocity.

We use colloidal solutions of silica (diameter of 5.5 and 2.0 μm , Micromod Partikeltechnologie GmbH, and 1.0 μm , Polysciences) and polystyrene (diameter of 5.7, 2.1, and 1.0 μm , Polysciences) diluted by deionized water to the appropriate concentration for each experiment. After sonication, the solution is directly dropped onto the prism; a 0.5-mm silicone spacer and glass substrate (Matsunami) are employed to enclose the sample solution. Figure 1(b) shows the Fourier-transform infrared spectra of the silica and polystyrene particles dropped and dried on a diamond prism. The absorption around the 9.3- μm wavelength range is ascribed to Si-O-Si asymmetric stretching [24], whereas there is no obvious absorption for the polystyrene particles.

III. THEORY

We calculate the optical force exerted on particles in the evanescent wave using two methods: Rayleigh

approximation for the 1- μm particles and finite-difference time-domain (FDTD) simulation for 1-, 2-, and 5.5- μm particles. First, we explain the Rayleigh approximation. The expression of time-averaged radiation force, \mathbf{F} , exerted on the particle is a function of electric field, \mathbf{E} , and induced polarization, \mathbf{P} , written as [13,14]

$$\langle \mathbf{F}(\omega) \rangle = (1/2)\text{Re} \int d\mathbf{r} [\nabla \mathbf{E}(\mathbf{r}, \omega)^*] \cdot \mathbf{P}(\mathbf{r}, \omega). \quad (1)$$

The evanescent wave propagated in x direction along the prism surface is expressed as [25]

$$\mathbf{E}(\mathbf{r}, \omega) = E_0 \exp(-\xi z) \exp i \left[\left(k_t \frac{n_i}{n_t} \sin \theta_i \right) x \right], \quad (2)$$

$$\xi = \frac{k_t}{n_t} (n_i^2 \sin^2 \theta_i - n_t^2)^{1/2}, \quad (3)$$

where E_0 is the electric field amplitude. k_t , n_i , n_t , and θ_i are the wave number in water solution, refractive indices of ZnSe, and water and the incident angle of the laser [see the configuration in the inset of Fig. 5(b)].

For the induced polarization, $\mathbf{P} = \alpha_{\text{CMRR}} \mathbf{E}$, we use the Clausius-Mossotti law including the radiative reaction effect as [26,27]

$$\alpha_{\text{CMRR}} = \frac{\alpha_{\text{CM}}}{1 - ik_t^3 \frac{\alpha_{\text{CM}}}{6\pi\epsilon_0\epsilon_2}}, \quad \alpha_{\text{CM}} = 4\pi r^3 \epsilon_0 \epsilon_2 \frac{\epsilon_1 - \epsilon_2}{\epsilon_1 + 2\epsilon_2}, \quad (4)$$

where $\epsilon_0, \epsilon_1, \epsilon_2$ are vacuum permittivity, dielectric constants of the particles and water solution. r is the particle radius. The refractive indices of silica and polystyrene at 9.3- μm wavelength are $2.24+i2.15$ [28] and $1.54+i0.028$ [29], respectively. By substituting Eqs. (2) and (4) into Eq. (1), the optical force exerted on the 1- μm particles around the prism surface can be calculated.

For the larger size of particles, we use finite-difference time-domain simulation (software, Ansys Lumerical FDTD). The plane propagating wave of 9.3- μm laser with the incident angle of 57° is irradiated to the interface of the ZnSe and water [see the configuration in the inset of Fig. 5(b)]. The direction of the polarization is the same as in the experiment. All the refractive indices used in the simulation are the same as that used for the Rayleigh approximation. The optical force is calculated by volume-integrating the sphere. The mesh size around the sphere is 25 nm. The optical force exerted on each particle is calculated by changing the z displacement, as shown in Fig. 5.

IV. RESULTS AND DISCUSSION

We now describe the representative results for the 5.5- μm silica particles in the 9.3- μm evanescent wave. Initially, the silica particles dispersed in water are precipitated

on the prism before laser irradiation because of gravity [see Fig. 2(a)]. When subjected to laser irradiation, the particles are pushed and drift along the direction of the k vector of the 9.3- μm evanescent wave as shown in Figs. 2(a)–2(c). As the laser beam diameter in the horizontal direction is approximately 200 μm , the entire region in the dark-field scattering image is irradiated.

To represent the particle motion continuously over time, we perform image processing to obtain the particle trajectory as depicted in Fig. 2(d) (the detailed process is explained in Sec. 1 within the Supplemental Material [30]). Before laser irradiation, the trajectories of the particles are almost unchanged because their Brownian motion is moderate. [0–10 s as shown in Fig. 2(d)]. When the laser is turned on, the particles drift along the light-propagating direction as observed in Fig. 2(d) where all the trajectories move to the right side of the image after 10 s. For instance, a particle travels approximately 130 μm within 50 s, and the average velocity with standard deviation is $2.7 \pm 0.64 \mu\text{m/s}$ among seven particles. In addition, the particles move relatively faster at the center of the image, which is near the focal center of the 9.3- μm laser beam. The slope of the trajectory corresponds to the velocity and is nearly constant, suggesting that the optical force and the drag friction force from the solvent are balanced. This indicates that the particles move at the terminal velocity, and the optical force can be simply estimated as $120 \pm 30 \text{ fN}$ by using the value of the viscosity of water ($0.89 \times 10^{-3} \text{ cP}$).

When silica particles are replaced by 5.7- μm polystyrene particles, they move very slowly compared to the silica particles [see Figs. 2(e)–2(h)]. Their trajectories are slightly biased to the right after laser irradiation. For example, the maximum distance traveled by a particle is 20 μm within 50 s. According to the slopes depicted in Fig. 2(h), the averaged velocity is $0.30 \pm 0.075 \mu\text{m/s}$, and the corresponding optical force is $14 \pm 3.6 \text{ fN}$. The optical force exerted on the silica particle is approximately 8 to 9 times higher than that on the polystyrene one.

Moreover, a similar enhancement is observed for silica particles at a smaller diameter of 2.0 μm as shown in Figs. 2(i)–2(p). Although particle fluctuation becomes vigorous due to Brownian motion, the 2.0- μm silica particles are strongly accelerated by the 9.3- μm evanescent wave. The average velocities of the 2.0- μm silica and 2.1- μm polystyrene particles are 2.0 ± 0.32 and $0.28 \pm 0.11 \mu\text{m/s}$, respectively. The corresponding forces are $34 \pm 5.4 \text{ fN}$ and $5.0 \pm 1.9 \text{ fN}$, respectively, and the enhancement factor is approximately seven. In addition, the least silica particle size employed in this study is 1.0 μm (see Sec. 2 within the Supplemental Material [30]). Briefly, the maximum velocity is 1.9 $\mu\text{m/s}$ (the corresponding optical force is 16 fN); drifting of the 1.0- μm polystyrene particles is not clearly observed because the random force arising from Brownian motion is stronger than the optical force. Besides, dark

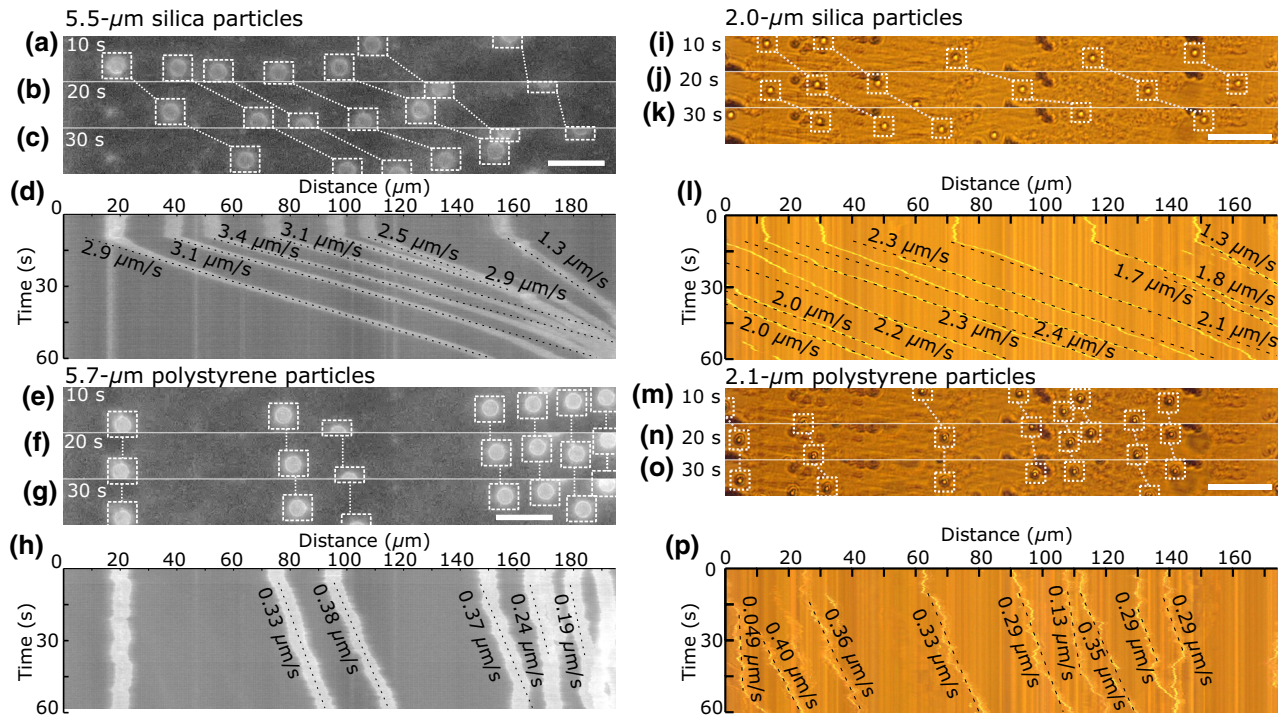


FIG. 2. Sequential images representing the movement of (a)–(c) 5.5- μm silica, (e)–(g) 5.7- μm polystyrene, (i)–(k) 2.0- μm silica, and (m)–(o) 2.1- μm polystyrene particles in the 9.3- μm evanescent wave. These particles are marked by white dotted squares connected by white dotted lines. The evanescent wave propagates along the prism surface from left-to-right in the images, and the laser is turned on at approximately 10 s. The length of the white bar is 20 μm . (d),(h),(l),(p) Image-processed pictures showing the respective trajectories of the silica and the polystyrene particles. The dashed-black slopes correspond to the velocity indicated nearby. The panel on the left depicts the scattering images, whereas that on the right depicts the transmission images.

shadows and vertical lines appear in the images due to surface roughness. Additionally, a few discontinuous trajectories are observed because the particles are framed-out and -in from the field-of-view.

We demonstrate that the velocity of particles can be controlled by NaCl addition. In Fig. 3, we summarize the velocity of 5.5- μm silica particles depending on the NaCl concentration. The velocity increases significantly from 0–100 $\mu\text{g/ml}$ and stagnated from 100–250 $\mu\text{g/ml}$. By adding sodium and chloride ions into the water solution, surface charges around the particles and the ZnSe prism surface are neutralized. Then, the repulsive electrostatic force between the particle and the surface becomes weaker, and their distance becomes closer. For instance, the colloidal particles tend to form clusters in the salt solution [31]. Namely, the particles are further penetrated into the evanescent wave, resulting in a larger optical force and observed velocity enhancement. Besides, in the high NaCl concentration (250 $\mu\text{g/ml}$), a lot of the particles are stuck to the prism surface, that suggests the repulsive electrostatic force becomes weaker as we mention above (the data in Fig. 3 shows only the particle in motion).

Regarding water heating by the laser, we did not observe any significant perturbation to the optical pushing in this

system. In general, the direction of the thermophoretic force is from hot to cold or vice versa depending on the Soret coefficient [32]. Therefore, the particle should move outward or toward the focal center, but not in one direction as observed. In addition, the particles may be heated from the bottom because they are on the evanescent

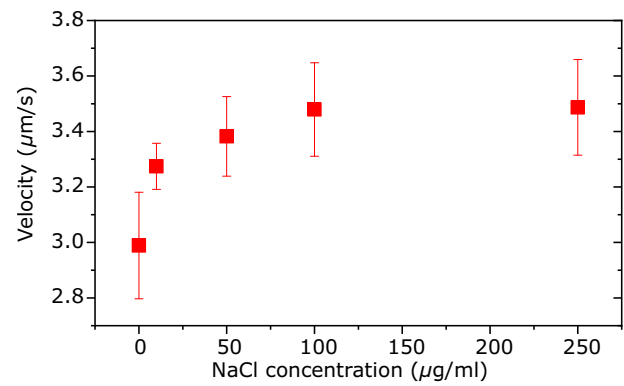


FIG. 3. The velocity of 5.5- μm silica particles in different NaCl concentrations. Each data point is obtained from 15 particles.

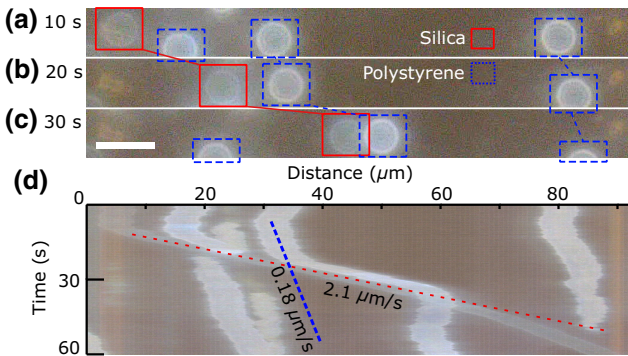


FIG. 4. (a)–(c) Sequential scattering images representing the movement of the 5.5- μm silica and 5.7- μm polystyrene particles in the mixture solution, in the 9.3- μm evanescent wave. These particles are marked by squares connected by lines. The laser propagates from left to right in the images, and is turned on at approximately 10 s. The length of the white bar is 10 μm . (d) Image-processed picture showing the respective trajectories, the silica, and polystyrene particles. The dashed thin-red and thick-blue slopes correspond to the respective velocities of the silica and polystyrene particles indicated nearby.

wave (the intensity profiles around each particle are simulated in Sec. 3 within the Supplemental Material [30]). However, the direction of the generated temperature gradient inside the particles is not equal to the direction in which the particles are pushed. Therefore, we argue that the self-thermophoresis mechanism [33,34] cannot explain this observation.

Next, we perform an experiment with a mixture solution of 5.5- μm silica and the 5.7- μm polystyrene particles to clearly demonstrate that silica particles can be selectively accelerated (see Fig. 4). We differentiate silica and polystyrene particles based on their brightness in the scattering images because the refractive index of the polystyrene is greater than that of silica in the visible wavelength region. In Fig. 1, the silica particles drift considerably faster than the others in the mixture solution (see also Video 1). In this case, in particular, the velocity of the silica particles (2.1 $\mu\text{m}/\text{s}$) is more than 10 times that of the polystyrene ones (0.18 $\mu\text{m}/\text{s}$). One of the features is the pushing of the polystyrene particle from behind by the silica particle [Fig. 1(c)]. However, when the polystyrene particle deviates from the course of the silica particle, it is no longer pushed as shown in Fig. 1(d) (after 30 s). Hence, we believe that silica particles can be optically filtered from a mixture solution, by preparing an optimized experimental setup with, for example, optofluidic microchannels.

To support the experimental data, we calculate the optical force exerted on each particle size in the evanescent field using Rayleigh approximation and the FDTD method. As shown in Fig. 5, the optical force (F_x) along the surface increases exponentially as the particle moves close to the



VIDEO 1. Video showing the movement of the 5.5- μm silica and 5.7- μm polystyrene particles in the mixture solution, in the 9.3- μm evanescent wave. The video is played at 5 \times speed.

surface (the gradient force along the z displacement is presented in Sec. 4 within the Supplemental Material [30]). The optical force exerted on the 1- μm , 2- μm , and 5.5- μm silica particles is 42.9, 173, and 530 fN, respectively, when the particles are on the surface, whereas that for the polystyrene particles is 1.17, 5.58, and 23.7 fN, respectively (see Table I). For the respective sizes, the forces acting on silica are enhanced by approximately 36.7, 31.0, and 22.4 times compared to polystyrene. In the calculation based on Rayleigh approximation, this enhancement factor is approximately 32, which is directly related to the imaginary part of the silica particle polarizability. The slight modulation from each enhancement factor may be due to Mie scattering. Thus, this force enhancement ascribes to vibrational resonant absorption.

In addition, the scaling of the force with the particle size exhibits a similar trend between the theoretical and experimental results. Comparing the 1- μm and 2- μm silica particles, the force is 3.4 times enlarged in the experiment, whereas it is enhanced 4.03 times in the FDTD simulation. Moreover, comparing the 1- μm and 5.5- μm silica particles, the increment factors are 12.0 and 12.4 in the experiment and simulation, respectively.

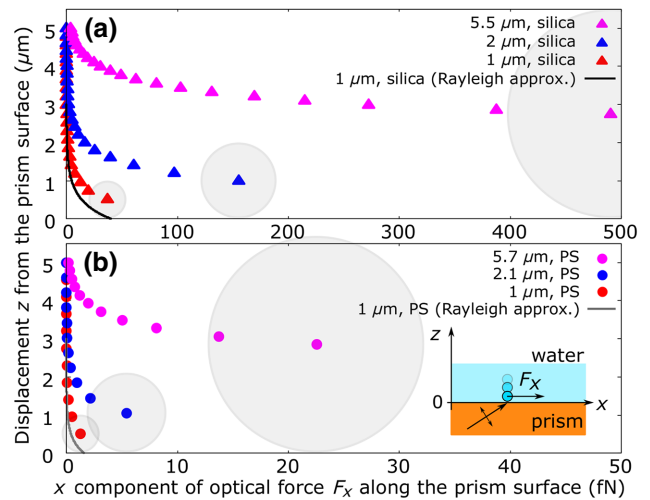


FIG. 5. Theoretical calculation of the optical force exerted on silica and polystyrene particles in the 9.3- μm evanescent wave. x component of the optical force as a function of the displacement from the prism surface for (a) silica and (b) polystyrene particles. The inset illustrations represent the particle coordinate configuration. The gray-shaded circles correspond to each particle scale. PS is an abbreviation for polystyrene.

TABLE I. Estimated optical force (fN). The force based on Rayleigh approximation is calculated at $z = 0$ (and $z =$ particle radius). PS is an abbreviation for polystyrene.

Particles	Experiment	FDTD	Rayleigh approx.
1.0 μm Silica	10 ± 4.3	42.9	40.3(13.5)
1.0 μm PS	...	1.17	1.61(0.42)
2.0 μm silica	34 ± 5.4	173	...
2.1 μm PS	5.0 ± 1.9	5.58	...
5.5 μm silica	120 ± 30	530	...
5.7 μm PS	14 ± 3.6	23.7	...

Regarding the difference in the absolute values between the experiment and simulation, the forces for the silica particles are nearly 5 times different, whereas those for polystyrene are in good agreement. This discrepancy is because the enhancement factors estimated based on the experiment (7–10 times) and theory (22–37 times) are moderately mismatched. This problem may be solved if the z displacement of the particles from the prism surface is accurately estimated by observing the intensity of the fluorescent dyes doped in the silica particles under visible evanescent-wave excitation, because the force responds exponentially to the z displacement. In addition, the friction force from the prism surface may need to be considered when estimating the optical force experimentally. Based on these theoretical facts, we believe that the observed phenomena are attributed to optical force enhanced by molecular vibrational resonance.

V. CONCLUSION

We demonstrate optical manipulation based on molecular vibrational resonance by introducing a midinfrared quantum cascade laser for optical manipulation experiment. We experimentally observe that the silica particles in the mixture solution are strongly and selectively pushed in the 9.3- μm evanescent wave, which excites their vibration mode in resonance. Although a relevant concept has recently been proposed in theoretical studies on the midinfrared optical force with graphene plasmonics [35,36], our finding presents the clear experimental evidence proving the concept of vibrational resonance. Traditionally, visible and near-infrared lasers have been commonly used in optical manipulation studies; Ashkin innovated optical tweezers [2] with near-infrared lasers transparent to biological cells. The significant laser absorption of water in the midinfrared region may be a technical and realistic concern for initiating experiments with midinfrared lasers. However, we realize these results utilizing an evanescent wave by having a hint from the attenuated total reflection method commonly used for the midinfrared spectral measurements of the liquid phase.

Apart from the electronic and vibrational resonant schemes, optical sorting has been reported using different

mechanisms such as whispering-gallery modes [37,38] and circular dichroism [39]. We expect that the net force will be further enhanced by integrating the vibrational resonance effects. Considering (i) the current extension of plasmonic research toward the midinfrared region [40], and (ii) the extensive development of plasmonic nano-optical tweezers in the visible and near-infrared regions in the past decade [3,4], we believe that midinfrared optical manipulation, with the aid of plasmonic techniques, can open an avenue for the mechanical control of nanoscopic matters (such as inorganic minerals, silicone polymers, and organic compounds) according to their infrared spectral information.

ACKNOWLEDGMENTS

This work is partially supported by Core Research for Evolutional Science and Technology (JPMJCR17N5), Japan Society for the Promotion of Science (KAKENHI, JP 21K14555), Inoue Foundation for Science (Inoue Science Research Award), and Toyota Physical and Chemical Research Institute (Toyota Riken Scholar).

- [1] A. Ashkin, Acceleration and Trapping of Particles by Radiation Pressure, *Phys. Rev. Lett.* **24**, 156 (1970).
- [2] A. Ashkin, J. M. Dziedzic, J. E. Bjorkholm, and S. Chu, Observation of a single-beam gradient force optical trap for dielectric particles, *Opt. Lett.* **11**, 288 (1986).
- [3] M. Righini, A. S. Zelenina, C. Girard, and R. Quidant, Parallel and selective trapping in a patterned plasmonic landscape, *Nat. Phys.* **3**, 477 (2007).
- [4] Y. Zhang, C. Min, X. Dou, X. Wang, H. P. Urbach, M. G. Somekh, and X. Yuan, Plasmonic tweezers: for nanoscale optical trapping and beyond, *Light Sci. Appl.* **10**, 59 (2021).
- [5] S. Kawata and T. Sugiura, Movement of micrometer-sized particles in the evanescent field of a laser beam, *Opt. Lett.* **17**, 772 (1992).
- [6] Y. Jiang, T. Narushima, and H. Okamoto, Nonlinear optical effects in trapping nanoparticles with femtosecond pulses, *Nat. Phys.* **6**, 1005 (2010).
- [7] D. G. Grier, A revolution in optical manipulation, *Nature* **424**, 810 (2003).
- [8] M. A. Osborne, S. Balasubramanian, W. S. Furey, and D. Klenerman, Optically biased diffusion of single molecules studied by confocal fluorescence microscopy, *J. Phys. Chem. B* **102**, 3160 (1998).
- [9] G. Chirico, C. Fumagalli, and G. Baldini, Trapped Brownian motion in single- and two-photon excitation fluorescence correlation experiments, *J. Phys. Chem. B* **106**, 2508 (2002).
- [10] T. Iida and H. Ishihara, Theoretical Study of the Optical Manipulation of Semiconductor Nanoparticles under an Excitonic Resonance Condition, *Phys. Rev. Lett.* **90**, 057403 (2003).
- [11] C. Hosokawa, H. Yoshikawa, and H. Masuhara, Enhancement of biased diffusion of dye-doped nanoparticles by

- simultaneous irradiation with resonance and nonresonance laser beams, *Jpn. J. Appl. Phys.* **45**, L453 (2006).
- [12] H. Li, D. Zhou, H. Browne, and D. Kleinerman, Evidence for resonance optical trapping of individual fluorophore-labeled antibodies using single molecule fluorescence spectroscopy, *J. Am. Chem. Soc.* **128**, 5711 (2006).
- [13] T. Kudo and H. Ishihara, Proposed Nonlinear Resonance Laser Technique for Manipulating Nanoparticles, *Phys. Rev. Lett.* **109**, 087402 (2012).
- [14] T. Kudo and H. Ishihara, Resonance optical manipulation of nano-objects based on nonlinear optical response, *Phys. Chem. Chem. Phys.* **15**, 14595 (2013).
- [15] M. Ploschner, T. Čižmár, M. Mazilu, A. Di Falco, and K. Dholakia, Bidirectional optical sorting of gold nanoparticles, *Nano Lett.* **12**, 1923 (2012).
- [16] S. E. Skelton Spesyvtseva, S. Shoji, and S. Kawata, Chirality-Selective Optical Scattering Force on Single-Walled Carbon Nanotubes, *Phys. Rev. Appl.* **3**, 044003 (2015).
- [17] M. L. Juan, C. Bradac, B. Besga, M. Johnsson, G. Brennen, G. Molina-Terriza, and T. Volz, Cooperatively enhanced dipole forces from artificial atoms in trapped nanodiamonds, *Nat. Phys.* **13**, 241 (2017).
- [18] H. Fujiwara, K. Yamauchi, T. Wada, H. Ishihara, and K. Sasaki, Optical selection and sorting of nanoparticles according to quantum mechanical properties, *Sci. Adv.* **7**, eabd9551 (2021).
- [19] R. Bresolí-Obach, T. Kudo, B. Louis, Y.-C. Chang, I. G. Scheblykin, H. Masuhara, and J. Hofkens, Resonantly enhanced optical trapping of single dye-doped particles at an interface, *ACS Photonics* **8**, 1832 (2021).
- [20] D. Rodrigo, O. Limaj, D. Janner, D. Etezadi, F. J. García de Abajo, V. Pruneri, and H. Altug, Mid-infrared plasmonic biosensing with graphene, *Science* **349**, 165 (2015).
- [21] J. Haas and B. Mizaikoff, Advances in mid-infrared spectroscopy for chemical analysis, *Annu. Rev. Anal. Chem.* **9**, 45 (2016).
- [22] M. R. Querry, Optical constants of minerals and other materials from the millimeter to the ultraviolet, Contractor Report CRDEC-CR-88009 (1987).
- [23] G. M. Hale and M. R. Querry, Optical constants of water in the 200-nm to 200- μm wavelength region, *Appl. Opt.* **12**, 555 (1973).
- [24] B. Stuart, *Infrared Spectroscopy: Fundamentals and Applications* (John Wiley & Sons, Ltd, England, 2004).
- [25] M. L. Martin-Fernandez, C. J. Tynan, and S. E. D. Webb, A ‘pocket guide’ to total internal reflection fluorescence, *J. Microsc.* **252**, 16 (2013).
- [26] B. T. Draine, The discrete-dipole approximation and its application to interstellar graphite grains, *Astrophys. J.* **333**, 848 (1988).
- [27] S. Albaladejo, M. I. Marqués, F. Scheffold, and J. J. Sáenz, Giant enhanced diffusion of gold nanoparticles in optical vortex fields, *Nano Lett.* **9**, 3527 (2009).
- [28] J. Kischkat, S. Peters, B. Gruska, M. Semtsiv, M. Chashnikova, M. Klinkmüller, O. Fedosenko, S. Machulik, A. Aleksandrova, G. Monastyrskyi, Y. Flores, and W. T. Maselink, Mid-infrared optical properties of thin films of aluminum oxide, titanium dioxide, silicon dioxide, aluminum nitride, and silicon nitride, *Appl. Opt.* **51**, 6789 (2012).
- [29] X. Zhang, J. Qiu, J. Zhao, X. Li, and L. Liu, Complex refractive indices measurements of polymers in infrared bands, *J. Quant. Spectrosc. Radiat. Transf.* **252**, 107063 (2020).
- [30] See Supplemental Materials at <http://link.aps.org/supplemental/10.1103/PhysRevApplied.18.054041> for image processing, 1- μm particles, intensity distribution around each particle, and gradient force toward the surface.
- [31] S.-F. Wang, T. Kudo, K. Yuyama, T. Sugiyama, and H. Masuhara, Reflection microspectroscopic study of laser trapping assembling of polystyrene nanoparticles at air/solution interface, *Langmuir* **32**, 12488 (2016).
- [32] S. Duhr and D. Braun, Why molecules move along a temperature gradient, *Proc. Natl. Acad. Sci. USA* **103**, 19678 (2006).
- [33] H.-R. Jiang, N. Yoshinaga, and M. Sano, Active Motion of a Janus Particle by Self-Thermophoresis in a Defocused Laser Beam, *Phys. Rev. Lett.* **105**, 268302 (2010).
- [34] X. Peng, Z. Chen, P. S. Kollipara, Y. Liu, J. Fang, L. Lin, and Y. Zheng, Opto-thermoelectric microswimmers, *Light Sci. Appl.* **9**, 141 (2020).
- [35] J. Zhang, W. Liu, Z. Zhu, X. Yuan, and S. Qin, Towards nano-optical tweezers with graphene plasmons: Numerical investigation of trapping 10-nm particles with mid-infrared light, *Sci. Rep.* **6**, 38086 (2016).
- [36] P. Paul and P. Q. Liu, Dynamically reconfigurable bipolar optical gradient force induced by mid-infrared graphene plasmonic tweezers for sorting dispersive nanoscale objects, *Adv. Optical Mater.* **10**, 2101744 (2022).
- [37] Y. Li, O. V. Svitelskiy, A. V. Maslov, D. Carnegie, E. Rafailov, and V. N. Astratov, Giant resonant light forces in microspherical photonics, *Light Sci. Appl.* **2**, e64 (2013).
- [38] Y. Li, A. V. Maslov, N. I. Limberopoulos, A. M. Urbas, and V. N. Astratov, Spectrally resolved resonant propulsion of dielectric microspheres, *Laser Photonics Rev.* **9**, 263 (2015).
- [39] G. Tkachenko and E. Brasselet, Optofluidic sorting of material chirality by chiral light, *Nat. Commun.* **5**, 3577 (2014).
- [40] T. Low and P. Avouris, Graphene plasmonics for terahertz to mid-infrared applications, *ACS Nano* **8**, 1086 (2014).